Microscopic and structural study on the formation of mechanochemical synthesized BaTiO$_3$ and ZnTiO$_3$ perovskites

GÁBOR KOZMA[1]* , DÁNIEL BERKESI[1], KATALIN LIPTAK[1], ANDREA RÓNAVÁRI[1], ÁKOS KUKOVECZ[1] and ZOLTÁN KÓNYA[1,2]

[1] Department of Applied and Environmental Chemistry, University of Szeged, H-6720, Szeged, Rerrich Béla Square 1, Hungary

[2] MTA, Reaction Kinetics and Surface Chemistry Research Group, H-6720, Szeged, Rerrich Béla Square 1, Hungary

ABSTRACT

In this work, the properties of mechanochemically produced (by using mills made from different materials) barium-titanate (BaTiO$_3$) and zinc-titanate (ZnTiO$_3$) perovskites are compared. Mechanochemistry is a process that can cover the energy demand of some reaction pathways between solid materials. This process is called "high-energy milling", for which not all types of mills are suitable. In our case, a planetary ball mill provided the necessary energy. Using a model, the required energy is determinable; the energy released during an impact of a milling ball (E_b – ball-impact energy), as well as during the whole milling (E_{cum} – cumulative milling energy). Thus, a milling-energy map was created, with which the applied E_b and E_{cum} values were visualized depending on the different grinding parameters. The parameters changed were the material of the grinding vessels, the number of grinding balls, and the rotational speed. The transformation was tracked by X-ray diffraction (XRD) measurements, and electron microscopic images (TEM and SEM) of the perovskites produced were taken. This study aimed to draw conclusions that will help later in the synthesis of materials with other perovskite structures by choosing optimal milling parameters.

INTRODUCTION

Mechanochemical reactions and mechanical activation in planetary ball mills have long been known. In the case of a planetary ball mill, there are several parameters that fundamentally influence these processes: the rotational speed; the material of the milling balls and vessel; the number of balls and the filling ratio of the balls and reactants; the milling time; the temperature and atmosphere in the vessel, the physical and chemical properties of the reactants etc. These parameters are not independent of each other and play an important role in achieving the best available yield. The value of ball-impact energy affects the increase in the particle size of materials, and as the temperature increases, compounds of different compositions may be formed [1]. For example, a long milling process can result in inadequate products, while too low milling energy does not allow for proper conversion of starting materials [2].

Due to its excellent properties, the group of chemical compounds with a perovskite structure includes a wide range of electrochemical materials: high-temperature superconductors, superionic conductors, and semiconductor dielectrics [3, 4]. The number of perovskites that can be produced by means of mechanochemistry is expanding. Our study aimed to explore the energy mapping of the process. Thereby, the mechanochemical perovskite synthesis can become a general process by which a large number of products can be prepared under laboratory conditions.

EXPERIMENTAL

Mechanochemical perovskite production was carried out using a Fritsch Pulverisette-6 planetary ball mill. Each experiment was conducted in grinding vessels with a volume of 80 mL. The material of the three different grinding vessels was: silicon-nitride (Si_3N_4), stainless-steel (FeNi) and tungsten-carbide (TC). The density of these vessels is $3.25\,g\,cm^{-3}$, $7.7\,g\,cm^{-3}$ and $14.3\,g\,cm^{-3}$, respectively. The excess energy generated by the density of the material thus approximately doubles by using harder grinding vessels. The grinding balls (10 mm in diameter) and 2.00 g of BaO with 1.04 g of TiO_2 or 1.50 g of ZnO with 1.47 g of TiO_2 were added to the vessel in each case. The explanation for this is that the total weight had to be kept at around 3 g. The number of grinding balls was changed between 10 and 25, while the rotational speed was changed between 300 and 500 rpm.

The energy equation (1) can be used to determine two energy values: the E_b (1), which represents the total energy available during an impact event of a milling ball, and E_{cum} (2), which means the energy transferred to 1 g of the powder during the whole milling process: [5].

$$E_b = \frac{1}{2}\varphi_b K \left(\rho_b \frac{\pi d_b^3}{6} \right) \omega_p^2 \left[\left(\frac{\omega_v}{\omega_d} \right)^2 \left(\frac{d_v - d_b}{2} \right)^2 \left(1 - 2\frac{\omega_v}{\omega_d} \right) \right.$$
$$\left. - 2r_p \left(\frac{\omega_v}{\omega_d} \right) \left(\frac{d_v - d_b}{2} \right) - \left(\frac{\omega_v}{\omega_d} \right)^2 \left(\frac{d_v - d_b}{2} \right)^2 \right] \tag{1}$$

where φ_b is the obstruction factor, K is the geometric constant of the instrument, d_b is the diameter of the balls, d_v is the diameter of the milling vessel, ρ_b is the density of the milling balls, ω_p and ω_v are the rotational speed of the disc and the vessel and r_p is the distance between the rotational axes of the disc and the vessel [6]. The value of K depends on the equipment (mill) and the diameter of the grinding balls. The value of the K is approximately 1.5 for ball diameters 10 mm, which can be used in most cases. [7] The equations (Eq. 1) fit quite well with the experimental measurements, and this confirms the usability of the model. Despite this in the case of the milling vessel being filled with milling balls above a certain number, a decrease in the value of E_b was observed. Therefore the hindering factor (φ_b), was introduced into the equation and the ball-impact energy was simply corrected. [5, 7] The value of φ_b varies from 1 to 0. In our case, depending on the number of grinding balls, its value varied from 0.98 (10 pcs) to 0.95 (25 pcs).

$$E_{cum} = \frac{E_b \times f \times t}{m_p} \tag{2}$$

where f is the frequency of impacts, t is the milling time and m_p is the mass of the sample. [6].

Powder X-ray diffraction patterns were obtained with a Rigaku Miniflex-II instrument operating with Cu-Kα radiation ($\lambda = 1.5406$ Å). The 2Θ Bragg angles were scanned over a range of 5–90° at a rate of $1.0°\,min^{-1}$. Transmission Electron Microscope (TEM) analysis was performed by an FEI-Tecnai G2/20/X-TWIN instrument with a point resolution of 0.26 nm. Samples were placed on holey carbon-coated copper grids of 300 mesh.

RESULTS AND DISCUSSION

Using the milling-energy model, the E_b values were determined with different settings. From these, a milling-energy map was created, which is shown in Fig. 1. It illustrates the relationship between E_b and the material of the applied vessel and between E_b and the rotational speed. In the case of FeNi and TC vessels, samples milled at 200, 300, 400, and 500 rpm are illustrated. Whereas, in the case of the samples milled in the silicon-nitride vessel, the conversion of the starting materials only started to take place at 300 rpm with 25 milling balls (200 rpm data are not shown). Figure 1 shows that in the case of higher density grinding vessel, increasing the rotational speed has a more significant impact on the dynamics of the growth of E_b. With the TC vessel, the minimum rotational speed will determine the applied energy resolution, nevertheless, a much wider energy spectrum can be achieved with it in contrast to the Si_3N_4.

Each grinding was performed for 3 h. Meanwhile, an hourly sample of the powder was taken, which was immediately measured by XRD. Figure 2 shows the XRD results of samples milled in different vessels with the same parameters ($\omega_d = 400$ rpm, $N_b = 20$ balls). As expected, the formation of both perovskites differs significantly in the three grinding vessels.

The typical reflections of $BaTiO_3$ between 2 theta 20–90° are listed below: 2 theta 22.1° (100); 31.5° (110); 38.8° (111); 45.1° (200); 50.7° (210); 56.1° (211); 65.7° (220); 70.2° (300); 74.7° (310); 78.9° (311). [8] $BaTiO_3$ produced at a sintering temperature above 1,000 °C, is typically tetragonal and changed to the hexagonal structure above 1,400 °C [9]. The typical reflections of $ZnTiO_3$ between 2 theta 20–90° are listed below: 2 theta 23.8° (101); 29.7° (012); 32.8° (104); 35.2° (110); 40.3° (113); 48.8° (024); 53.3° (116); 56.5° (018); 61.8° (214); 63.1° (300). The $ZnTiO_3$ exhibits a pure crystalline phase of hexagonal [10].
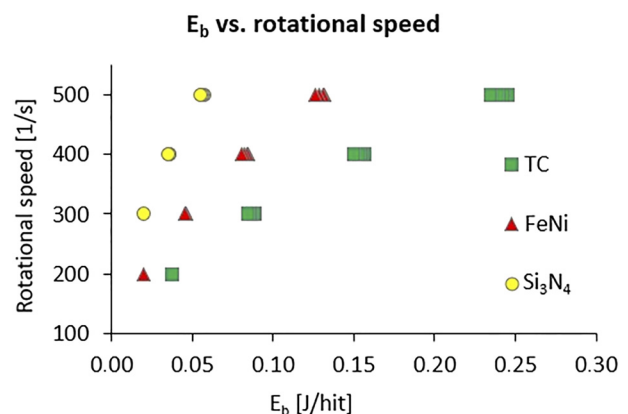

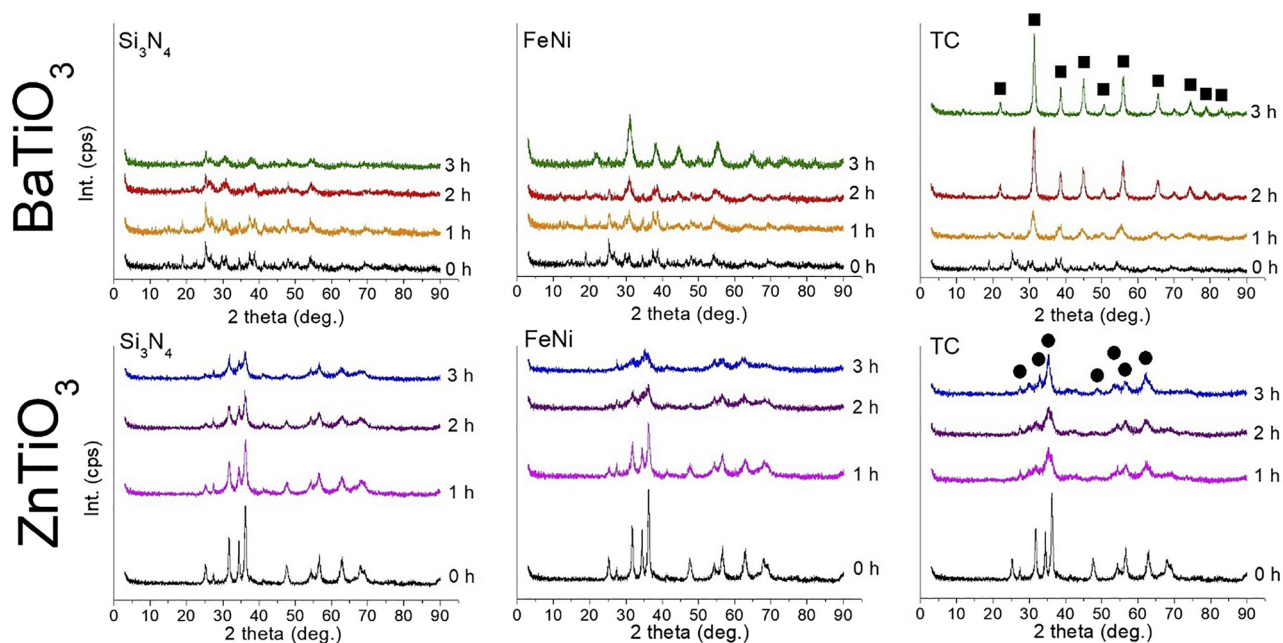Fig. 1. E_b points are defined by Eq. 1 as a function of the rotational speed (ω_p)

Fig. 2. Results of XRD measurements. The 0-h sample means the BaO/ZnO-TiO$_2$ starting materials mixture. ■ typical reflections of BaTiO$_3$ perovskite. ● typical reflections of ZnTiO$_3$ perovskite

The E_b can double depending on the material of the grinding vessel. This is well reflected in the XRD results. The production of BaTiO$_3$ is already sufficient at a lower E_b value, resulting in 35.5 mJ/hit. After 60 min typical reflections appear during treatment in the case of the FeNi grinding vessel. The transformation of precursors in the Si$_3$N$_4$ grinding vessel does not take place at this E_b value in the case of ZnTiO$_3$. The characteristic reflections of crystalline ZnTiO$_3$ appear only after 2 h in the FeNi milling vessel.

For the same samples, transmission electron microscopic measurements were also performed

Figures 3 and 4 shows the TEM images of BaTiO$_3$ and ZnTiO$_3$, respectively. It is clear that by increasing the density of the grinding vessels, i.e., the E_b, the morphology of the particles becomes sharper for both perovskites. While only a mixture of starting materials can be seen in the Si$_3$N$_4$ grinding vessel, as confirmed by the XRD results, individual particles can be distinguished in the samples made in the FeNi grinding vessel.

In the case of FeNi grinding vessels, the presence of synthesized perovskite and the mixture of starting materials are present at the same time, especially in the case of ZnTiO$_3$ (Fig. 4b). Separate particles of both BaTiO$_3$ and ZnTiO$_3$ can already be observed in the TC grinding vessel. The size of the particles falls within the nanoscale.

With the microscopic images, size distribution histograms were made of the samples synthesized in the stainless-steel and tungsten-carbide grinding vessels (Fig. 5). Due to the high-energy milling, crystal growth is inhibited during the formation of the perovskite structure, so the size of individual particles falls within the nano range. The conspicuous difference between the material produced in the two
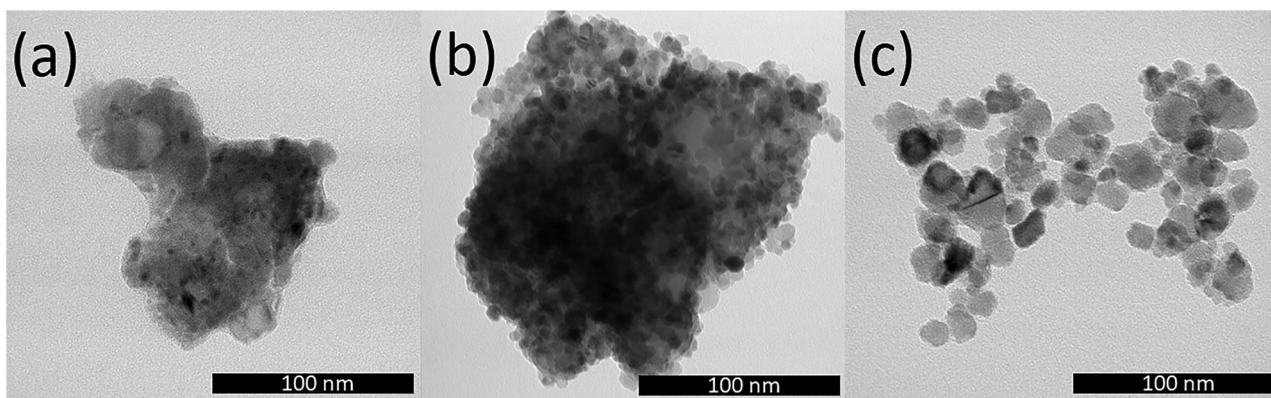

Fig. 3. TEM images of BaTiO$_3$ perovskites synthesized in the (a) Si$_3$N$_4$, (b) FeNi and (c) TC grinding vessels
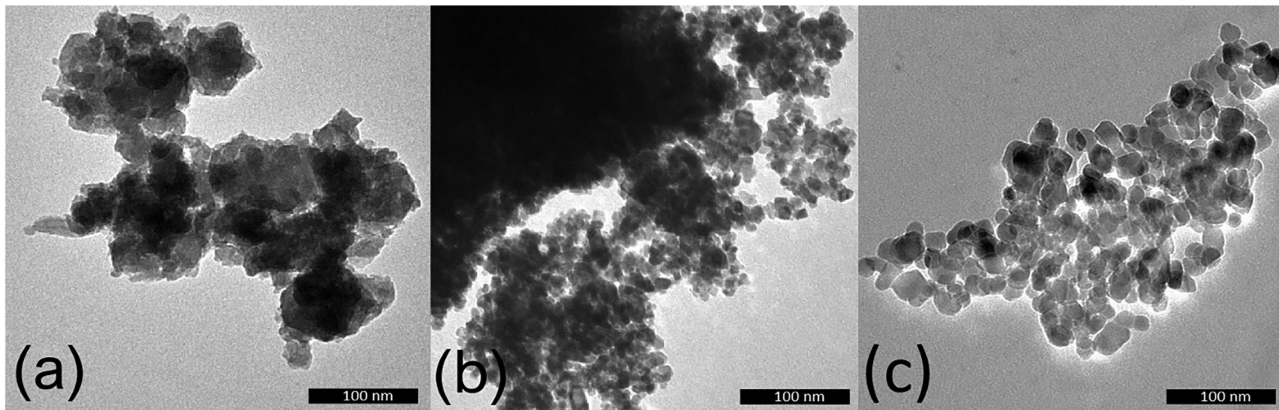
Fig. 4. TEM images of ZnTiO$_3$ perovskites synthesized in the (a) Si$_3$N$_4$, (b) FeNi and (c) TC grinding vessels

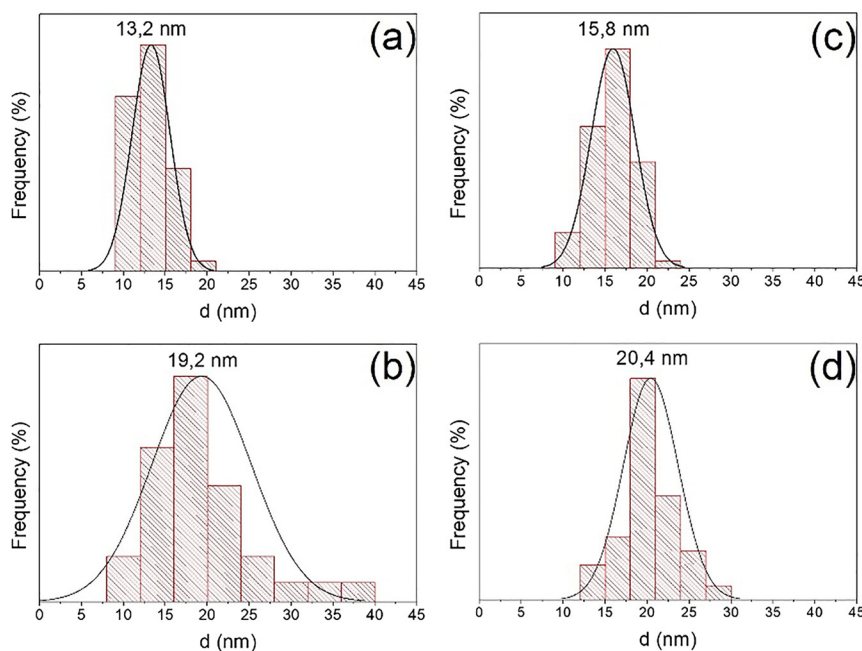*Fig. 5.* Histograms of the particle size distribution of BaTiO$_3$ (a, b) and ZnTiO$_3$ (c, d) perovskites produced in the FeNi (a, c) and TC (b, d) grinding vessels

grinding vessels is that the increase in particle size was measurable in the TC vessel, which provides more impact energy (E_b). This can be explained by the sintering caused by excess energy, which creates ever-larger particles by merging smaller separated particles. Overall, the average diameter of the perovskite particles is 14.5 and 19.8 nm.

CONCLUSION

For both perovskites, the formation of the structure can be achieved mechanochemically in a similar energy range. From this, we can conclude that the experience gained during the research can already be used to produce perovskites from the components of metal oxide.

As a result, it can be a general mechanochemical perovskite synthesis model: with adequate E_b, all three grinding vessels are suitable for the production of perovskites, while only the harder stainless steel and tungsten-carbide grinding drums are capable of the formation of nanoscale particles.

REFERENCES

1. Sopicka-lizer, M. Introduction to mechanochemical processing. In High-Energy Ball Milling; Elsevier, **2010**; pp 1–5.

2. Kozma, G. Examination of Mechanochemical Production and Modification Possibilities of Nanostructures; University of Szeged: Szeged, **2017**.

3. Vijatović, M.; Bobić, J.; Stojanović, B. History and Challenges of Barium Titanate: Part I; Science of Sintering, **2008**.

4. Stojanovic, B.; et al. Mechanochemical synthesis of barium titanate. *J. Eur. Ceram. Soc.* **2005**, *25*(12), 1985–9.

5. Burgio, N.; Iasonna, A.; Magini, M.; Martelli, S.; Padella, F. Mechanical alloying of the fe-zr system - correlation between input energy and end-products. *Nuovo Cimento Della Societa Italiana Di Fisica D-Condensed Matter At. Mol. Chem. Phys. Fluids Plasmas Biophys.* **1991**, *13*(4), 459–76.

6. Kozma, G.; et al. Experimental validation of the Burgio-Rojac model of planetary ball milling by the length control of multiwall carbon nanotubes. *Carbon* **2016**, *105*, 615–21.

7. Magini, M.; Iasonna, A.; Padella, F. Ball milling: an experimental support to the energy transfer evaluated by the collision model. *Scripta Mater.* **1996**, *43*(1), 13–9.

8. Siddheswaran, R.; Šutta, P.; Novák, P.; Netrvalová, M.; Hendrych, A.; Životský, O. In-situ X-ray diffraction studies and magneto-optic Kerr effect on RF sputtered thin films of $BaTiO_3$ and Co, Nb co-doped $BaTiO_3$. *Ceramics Int.* **2016**, *42*(3), 3882–7.

9. Sun, Q.; Gu, Q.; Zhu, K.; Jin, R.; Liu, J.; Wang, J.; Qiu, J. Crystalline Structure, Defect Chemistry and Room Temperature Colossal Permittivity of Nd-doped Barium Titanate. *Sci. Rep.* **2017**, *7*, 42274–42274.

10. Jain, P. K.; Kumar, D.; Kumar, A.; Kaur, D. Structural, optical and dielectric properties of $ZnTiO_3$ ceramics. *Optoelectronics Adv. Mater.* **2010**, *4*(3), 299–304.